HEFAT2011
8th International Conference on Heat Transfer, Fluid Mechanics and Thermodynamics
11-13 July 2011
Pointe Aux Piments, Mauritius

NUMERICAL STUDY OF EFFECT OF DESIGN AND PHYSICAL PARAMETERS ON A PEM FUEL CELL PERFORMANCE

S. O. Obayopo, T. Bello-Ochende* and J. P. Meyer
*Author for correspondence
Department of Mechanical and Aeronautical Engineering,
University of Pretoria,
Pretoria 0002,
South Africa.

ABSTRACT

A proton exchange membrane (PEM) fuel cell is one of the widely researched fuel cell systems due to its low temperature operation, high power density, fast start-up, system robustness and low emission characteristics. A three-dimensional numerical computation of the effect of design parameters (geometry and flow orientation) and physical parameters (gas diffusion layer porosity) on PEM fuel cell performance was carried out. The continuity, momentum, energy and species conservation equations describing the flow and species transport of the gas mixture in the coupled gas channels and the electrodes were numerically solved using a computational fluid dynamics code. This paper investigated how channel geometries (width and depth), flow orientation and gas diffusion layer (GDL) porosity affect performance and species distribution in a typical fuel cell system. The study also incorporated pressure drop characteristics in the flow channel. The numerical results computed agree well with experimental data in the literature.

Key words: PEM fuel cell; design parameters, physical parameters; computational fluid dynamics, performance

INTRODUCTION

A proton exchange membrane fuel cell (PEMFC) using hydrogen is one of the emerging fuel cells with many advantages ranging from emission of water as waste, operation at low temperature for quick start-up, and use of solid polymer as electrolytes, reducing both construction and safety complications. This fuel cell type is being highly considered as an alternative power source for stationary and mobile applications though with several technical challenges [1]. Model developments paved ways for the improvement of these new energy systems especially in the area of cost reduction. Fuel cell modelling received tremendous attention in the last two decades with the ultimate aim of better understanding of the underlying phenomenon during the working operation of fuel cells. For optimum performance of the fuel cell system, good distribution of the reactants throughout the stack is necessary. Also, minimisation of the pressure drop in the flow channel plays a prominent role in reducing the pumping power requirement of the fuel cell. The most prominent earlier works on PEMFC were from Bernardi [2], Bernardi and Verbrugge [3] and Springer *et al.* [4] which are based on one-dimensional models. Studies on fundamental issues of the PEM fuel cell system, including water management, have greatly advanced [5]. However, effect of flow field design on PEM fuel cells has received less attention [6]. Shimpalee *et al.* [7] studied the impact of channel length on PEMFC flow field design and obtained results showing the impact of channel length on local temperature, water content, and current density for a serpentine flow field. Greenway *et al.* [8] used a two-phase flow, non-isothermal model to study 10 cm^2 serpentine laboratory-scale flow field patterns with different flow path lengths and inlet/outlet configurations to study cell performance and distribution uniformity. Experimentally, Li *et al.* [9] compared a serpentine pattern with a matrix of individual graphite squares to see the effect on performance. Flow field design is still classified information in the fuel cell industry and, currently, there is no established design pattern [10]. Hence, there is need for more research tailored towards efficient flow field design.

One of the essential requirements in PEM fuel cells is efficient and uniform distribution of the reactant gases over the electrodes to minimise the concentration over potential and to subsequently improve power obtained from the cell. The effective design and optimisation of the gas flow fields remain one pertinent explored area for reasonable cost reduction and optimum performance attainment for PEM fuel cells, which is studied in this work. The model developed predicts the fuel cell performance under different channel geometries (width and height), GDL porosities and flow orientation. Results also

NOMENCLATURE

A_c	[m^2]	cross-sectional area
C_i	[kg kg^{-1}]	mass fraction of chemical species
C_p	[J kg^{-1} K^{-1}]	constant pressure heat capacity
D_h	[m]	hydraulic diameter
D_i^{eff}	[m^2 s^{-1}]	effective diffusion coefficient of species *i*
E_{OCV}	[V]	open-circuit voltage
F	[$Cmol^{-1}$]	Faraday constant (96,487 C mol^{-1})
f		friction factor
h_{react}	[J $Kmol^{-1}$]	enthalpy of electrochemical reactions
h_L	[J kg^{-1}]	enthalpy of condensation/vaporization of water
I	[A m^{-2}]	exchange current density
i_o	[Am^{-2}]	local current density
L	[m]	length
$\dot{m}$	[$kgs^{-1}m^{-2}$]	mass flow rate
n		electron number
p	[Pa]	pressure
R	[mol^{-1} K^{-1}]	universal gas constant (8.314J mol^{-1} K^{-1})
Re		Reynolds number
R_{ohm}	[Ω m]	ohm resistivity
$R_{an,\,cat}$	[A m^{-3}]	volumetric transfer current at anode and cathode
S		source term
t	[s]	time
T	[K]	temperature
V	[V]	cell voltage
V_{avrg}	[m/s]	mass- averaged velocity
v	[m/s]	components of velocity
x, y, z	[m]	coordinate

Greek symbols

α_{an}		electrical transfer coefficient (anode)
α_{cat}		electrical transfer coefficient (cathode)
β	[m^2]	permeability
μ	[kg m^{-1} s^{-1}]	fluid viscosity
ε		porosity of porous media
η	[V]	overpotential
λ^{eff}		effective heat conductivity
μ^{eff}	[kg s m^{-2}]	effective dynamic viscosity
Φ	[V]	phase potential function
ρ	[kg m^{-3}]	density

Subscripts and superscripts

an	anode
cat	cathode
e	electrolyte
O_2	oxygen
H_2	hydrogen
H_2O	water
i	species
m	mass
ohm	ohmic
ref	reference value
s	electronic conductive solid matrix
u	momentum
z	species value at reaction sites for 0,1,2,3 domains of the cell

highlight pressure drop characteristics in the species flow channel.

MODEL DEVELOPMENT

In the modelling of the fuel cell, the following assumptions were made: the cell operates under steady-state condition, isothermal boundary conditions were used for external walls, flow in the cell is considered to be laminar, reactants and products are assumed to be ideal gas mixtures, and the electrode is assumed to be an isotropic and homogeneous porous medium. Figure 1 shows a schematic diagram of a PEM fuel cell cross-section showing different zones and species transport across the zone. The physical dimensions of the fuel cell model at base case are summarised in Table 1. Table 2 is a summary of the base case operating conditions.

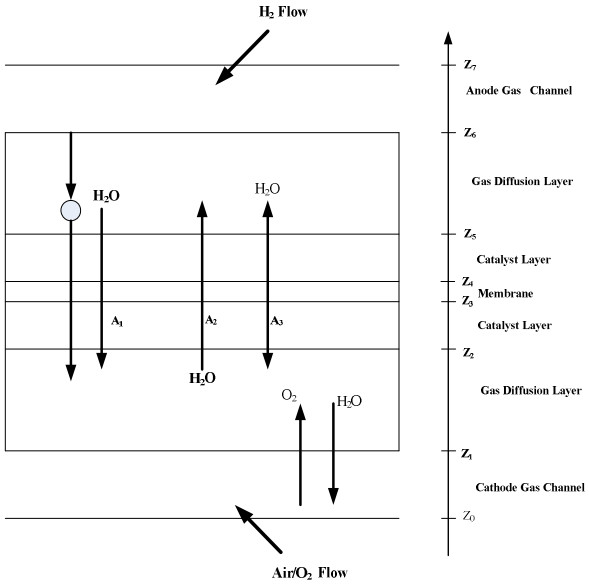

Figure 1 Schematic diagram of a PEM fuel cell showing different zones and species transport across the zone. Net water flux is the sum of: (A_1) electro-osmotic effect, (A_2) diffusion effect and (A_3) permeability effect.

The channel width was varied from 0.6 to 1.6 mm resulting in 6 cases (0.6, 0.8, 1.0, 1.2, 1.4, 1.6), while the channel depth was varied from 0.5 to 3.0 mm (0.5, 1.0, 1.5, 2.0, 2.5, 3.0). The channel length was fixed at 100 mm and pure hydrogen and air were used in the model. Figures 2 (a) and 2 (b) show the schematic diagram of the two flow configurations investigated (co-flow and counterflow) to study the effect of species flow orientation on the performance of the fuel cell system. The GDL porosities were varied from 0.1 to 0.7.

Table 1 Physical dimensions of the straight channel fuel cell section

Channel length (mm)	100
Channel width (mm)	0.6
Channel depth/height (mm)	0.8
Membrane thickness (mm)	0.036
Catalyst layer thickness (mm)	0.012
Electrode thickness (mm)	0.21

Table 2 Base case operating conditions

Cell operating temperature (^oC)	70
Air-side/fuel-side inlet pressure (atm)	3/3
Open-circuit voltage (V)	0.75
O_2 stochiometry ratio	1.2
H_2 stochiometry ratio	2.0
Permeability (m^2)	1.76 x 10^{-11}
Relative humidity of inlet fuel/air	100%
Reference current density of anode (A/m^2)	7 500
Reference current density of cathode (A/m^2)	20

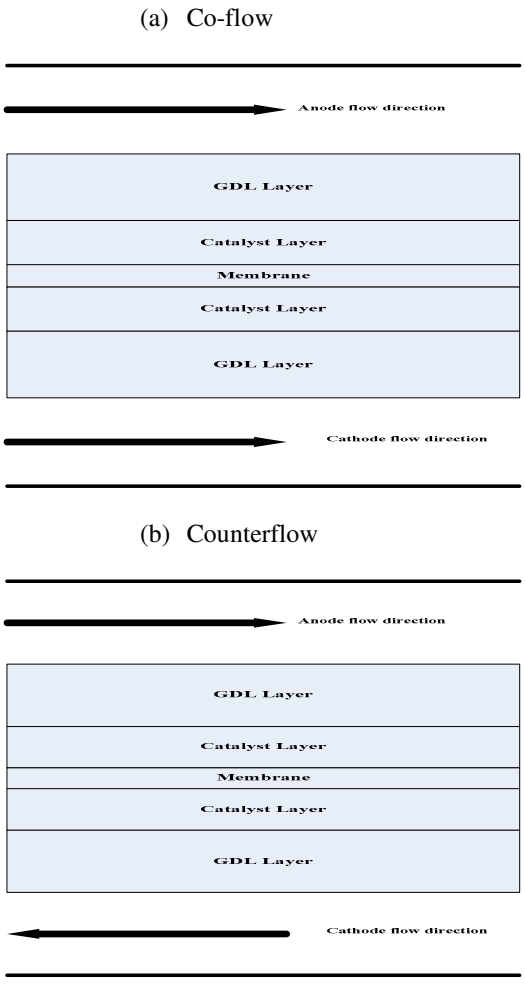

Figure 2 Schematic drawing of (a) co-flow orientation and (b) counterflow orientation.

2.1 Model equations

The basic transport equation (conservation of mass and momentum) applies to the transport of gas mixtures in the gas channels in the fuel cell. The corresponding governing equations are as follows:

Continuum equation:

$$\frac{\partial(\varepsilon\rho)}{\partial t} + \nabla\cdot(\varepsilon\rho u) = S_m \tag{1}$$

Momentum equation:

$$\frac{\partial(\varepsilon\rho u)}{\partial t} + \nabla\cdot(\varepsilon\rho uu) = -\varepsilon\nabla p + \nabla\cdot(\varepsilon\mu^{eff}\nabla u) + S_u \tag{2}$$

Species conservation equation:

$$\frac{\partial(\varepsilon\rho c_i)}{\partial t} + \nabla\cdot(\varepsilon\rho u c_i) = \nabla\cdot(-\rho D_i^{eff}\nabla c_i) + S_i \tag{3}$$

Energy conservation equation:

$$\frac{\partial(\rho C_p T)}{\partial t} + \nabla\cdot(\rho u C_p T) = \nabla\cdot(\lambda^{eff}\nabla T) + S_T \tag{4}$$

The energy source term, S_T, depicts the sum of the reversible heat release and the irreversible heat generation [11]. In the catalyst layer, the reversible and irreversible reaction heats as well as latent heat of water phase change are considered; for the membrane, ohm heating of current due to large resistance of the membrane is also considered. The total source that is accounted for in the thermal energy equation is:

$$S_T = h_{react} - R_{an,cat}\eta_{an,cat} + I^2 R_{ohm} + h_L \tag{5}$$

where h_{react} is net enthalpy change due to the electrochemical reactions, $R_{an,cat}\eta_{an,cat}$ is the product of the transfer current and the overpotential in the anode or the cathode catalyst layer, R_{ohm} is the ohmic resistivity of the conducting media, and h_L *is* the enthalpy change due to condensation/vaporisation of water. The source terms account for situations when a fluid passes through a porous medium. In this paper, the term is applicable to the electrode and catalyst zones. For low velocities encountered in fuel cells, these source terms are applicable at the gas diffusion layers and are given by Darcy's law:

$$S_{px} = -\frac{\mu v_x}{\beta_x}; \tag{6}$$

$$S_{py} = -\frac{\mu v_y}{\beta_y}; \tag{7}$$

$$S_{pz} = -\frac{\mu v_z}{\beta_z}; \quad \text{at } z_1 \le z \le z_6 \tag{8}$$

where μ is the fluid viscosity in the medium and β is the permeability of the electrode material. The permeability of the medium was assumed to be isotropic in this model hence; β_x, β_y and β_z all have the same value (1.76 x 10^{-11} m^2). Other source terms for the equations above used in the model were taken from [12]. The local current density i_o is a measure of the electrochemical reaction rate and generally given by the Butler-Volmer equation:

$$i_o = i_{o,ref}\left\{\exp\left[\frac{\alpha_{an} nF}{RT}\eta\right] - \exp\left[\frac{-\alpha_{cat} nF}{RT}\eta\right]\right\} \tag{9}$$

where η is the overpotential and defined as,

$$\eta = \left(\Phi_s - \Phi_e\right) - E_{ocv} \tag{10}$$

F is the Faraday constant, α_{an} and α_{cat} represent the experimental anodic and cathodic transfer coefficients, respectively; and R is the universal gas constant. For internal flows such as the ones in fuel cell channels, Reynolds number is conventionally defined as [13]

$$ReD_h = \frac{Inertial\ force}{Viscosity} = \frac{\rho V_{avr} D_h}{\mu} \tag{11}$$

where ρ is the density, μ the viscosity of the gas in the flow channel and *V is* the mass-averaged velocity in the flow channel determined by

$$V = \frac{\dot{m}}{\rho A_c} \tag{12}$$

$\dot{m}$ is the mass flow rate in the channel and D_h is the hydraulic diameter of the channel. For a rectangular channel in this study, D_h is defined as [13]

$$D_h = \frac{4A_c}{P^*} \tag{13}$$

where A_c is the cross-sectional area and P^* is the wetted perimeter of the gas flow channel. For the channel under consideration in Figure 3, the cross-sectional area is equal to the product of the side length

$$A_c = ab \tag{14}$$

and the wetted perimeter is

$$P^* = 2(a + b) \tag{15}$$

The pressure drop for a flow in a channel of length L is usually expressed using the following relation:

$$\Delta p = f\frac{L}{D_h}\frac{\rho V^2}{2} \tag{16}$$

where the friction factor *f* for steady fully developed laminar flows in a channel with square cross-section is given as [13]

$$f = \frac{56.91}{Re_{D_h}} \tag{17}$$

Substituting the above relation Eq. (17) into Eq. (16), and taking into consideration Eqs. (11) to (15), the pressure drop can be obtained for flow channels with square cross-section (a = b), as

$$\Delta P = 28.455\left(\frac{\mu\dot{m}}{\rho}\right)\left(\frac{L}{a^4}\right) \tag{18}$$

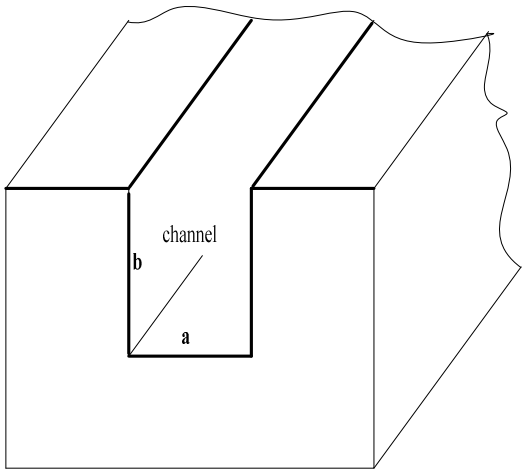

Figure 3 Channel cross-sectional view.

Thus the flow channel length for flow channels with a square cross-section can be determined as

$$L = \frac{\Delta p \rho a^4}{28.455\mu\dot{m}} \tag{19}$$

Similarly, we can obtain the flow channel length for a rectangular cross-section as

$$L = \frac{8\Delta p \rho (ab)^3}{C\mu\dot{m}(a+b)^2} \tag{20}$$

where $C = fReD_h$ is a function of the b/a for rectangular flow channels [13].

The pressure drop in the channel can be obtained using the flow rate (q) – pressure drop ΔP relationship for a rectangular cross-section relation [14]:

$$q = \frac{4ba^3}{3\mu} \times \frac{-\Delta P}{\Delta x}\left[1 - \frac{192}{\pi^5 b}\sum_{i=1,3,5..}^{\infty} \frac{\tanh\,(i\pi b/2a}{i^5}\right] \qquad (21)$$

Eq. (21) will allow the study of the pressure drop in the flow channel in the fuel cell.

BOUNDARY CONDITIONS

The inlets are all assigned as mass flow inlets. The gas diffusion layer and the catalyst layer are surrounded by sealed plates at the inlet and outlet plane, so the boundary conditions at the inlet and outlet planes take the no-slip condition for the velocity and non-permeable condition for the species mass fraction. The membrane-electrode interface is defined as a wall, primarily to inhibit species and electron crossover through the membrane. These also prevent pressure problems at this interface. In the areas at which the gas diffusion electrodes are in contact with the bipolar plates, a constant reference voltage equal to zero is assigned as a boundary condition both at the anode and at the cathode. The electron flux is set to zero at all other walls. The anode is grounded (V = 0) and the cathode terminal is set at a fixed potential less than the open-circuit potential. Both anode and cathode terminals are assigned wall boundary. The mass flow inlet of the hydrogen reactant gas at the anode channel was kept constant at 6.0×10^{-7} kg/s.

SOLUTION METHODOLOGY

The model equations were solved using commercial computational fluid dynamics (CFD) software ANSYS Fluent® 12.0 with Gambit® (2.4.6) as a pre-processor. The software has an add-on package for fuel cells, which has the requirement of the source terms for species transport equations, heat sources and liquid water formations [15]. Control volume technique was used for solving the problem. The meshes are more refined at the membrane/catalyst assembly regions. The conservation of mass, momentum and energy equations in the three-dimensions was solved, in turn, until the iterative process met the convergence criteria. In this study, definition of convergence criteria indicates that the largest relative error between two consecutive iterative residuals within the overall computational domains is less that 10^{-6}.

The domain was divided into hexahedral volume elements. A computational mesh of about 257 346 volume elements was obtained with the grid. The grid independence was verified at the preliminary test runs. Four structured grid configurations were evaluated for the PEMFC. The number of elements in the *x*-, *y*-, and *z*- directions was: (a) 70 × 70 × 25, (b) 87 × 87 × 34, (c) 104 × 87 × 34 and (d) 104 × 104 × 43. The influence of the number of elements on the local current density at operating voltage of 0.4 V was investigated. The local current density for grid (a) differs from that of (b-d) with deviation of about 4.2%. However, the local current density distributions for grids (b), (c) and (d) do not show any significant differences. The difference between the local current densities for (b) and (c) is about 0.36% and the difference between (c) and (d) is 0.48%. Grid (c) was chosen for the simulations as trade-offs between accuracy and cost of time. The solution strategy is based on the SIMPLE algorithm [16].

The simulation for each operating potential converged in 45 - 60 minutes depending on the current density on an Intel® Pentium dual-core processor T2390 1.86 GHz PC with 160 GB of HDD.

MODEL VALIDATION

The validation of physical and numerical models is very important; hence comparison with some experimental data is highly desirable. For fuel cell performance description, the polarisation curve or voltage-current curve is one of the most important final outcomes of numerical simulation and is widely used for validation purposes [17]. The simulation results for the base case operating conditions were verified against measurements of Wang *et al.* [18] and Cheng *et al.* [19]. The computed polarisation curve shown in Figure 4 is in good agreement with the experimental curves in the low load region. However, the model current density in the high mass transport limited region (> 2.75 A/cm^2) is higher than the experimental values. This observation is common in models where the effect of reduced oxygen transport due to water flooding at the cathode at higher current density cannot be properly accounted for [20].

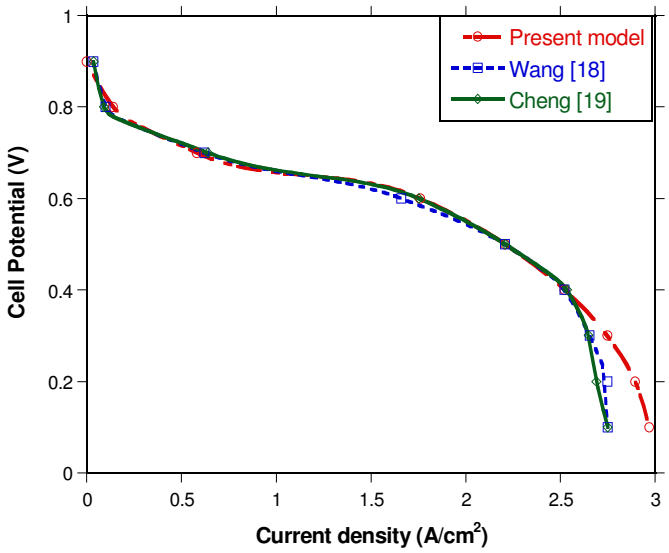

Figure 4 Comparison of model prediction and experimental polarisation curves at base condition.

RESULTS AND DISCUSSION

Pressure drop in flow channel

Figure 5 shows the pressure drop characteristics at a temperature of 70 ^{0}C. The result shows that the pressure drop increased as the flow rate at the cathode (air-side) is increased. This is expected since increase in flow rate increases the reaction of the reactant species and also reduces the resident water in the cathode channel of the PEMFC. Generally, fuel cells with high pressure loss in the flow field exhibit a more even distribution of the reactant species flow than those with

low pressure loss in their flow field. These even distributions do greatly enhance the fuel cell performance.

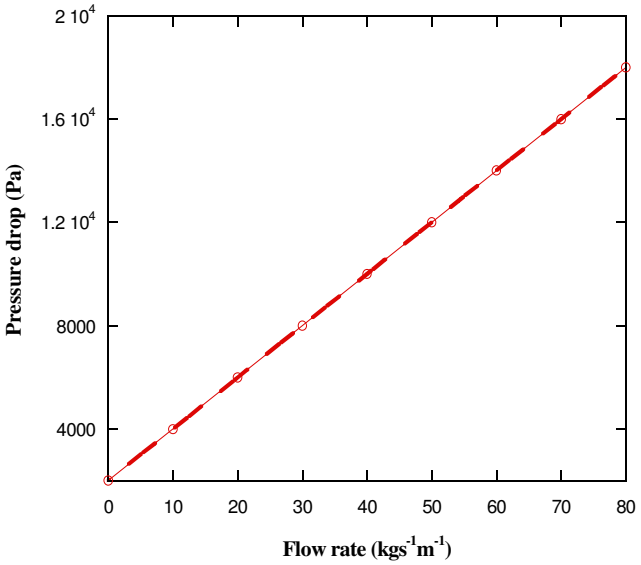

Figure 5 Pressure drop along the model flow channel at base operating conditions for channel depth 2.0 mm and width 1.2 mm.

Effect of channel geometry

Simulations were performed for different sets of channel dimensions. Two different parameters viz. channel width and channel depths were chosen for the study. Figure 6 illustrates the effect of channel depth on the fuel cell performance at constant channel length. The optimal current density for the fuel cell was obtained at a channel depth of 2.0 mm (current density: 2.62 A/cm^2). Further increase in depth showed a decline in fuel cell performance. Figure 7 shows the fuel cell performance for the six cases of channel width considered. Performance increased gradually from case 1 (0.6 mm – current density: 1.30 A/cm^2) until an optimum was obtained at case 4 (1.2 mm – current density: 2.45 A/cm^2). Increasing the channel width beyond 1.2 mm showed a reduction in fuel cell performance. These results were consistent with those observed by other researchers in their work. Watkins *et al.* [21] studied optimal dimension for cathode-side channel of fuel cells. They claimed the most preferred ranges to be 1.02 - 2.04 mm for channel depth and 1.14 - 1.4 mm for channel width.

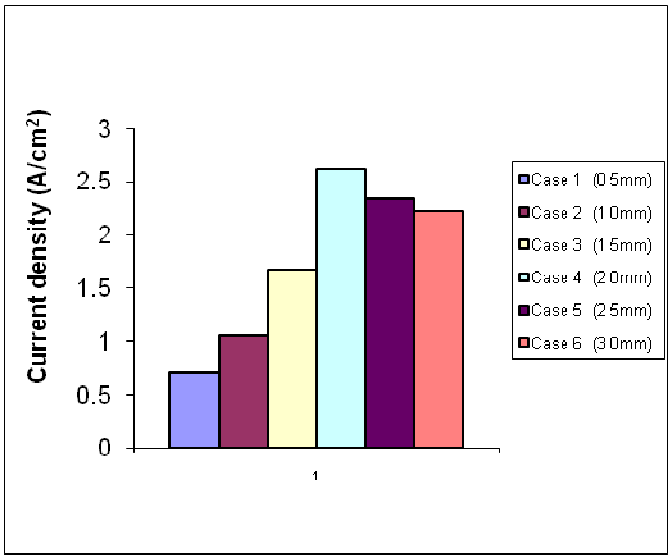

Figure 6 Current density obtained at different channel depth at cell potential 0.4 V and temperature 70 ^{0}C.

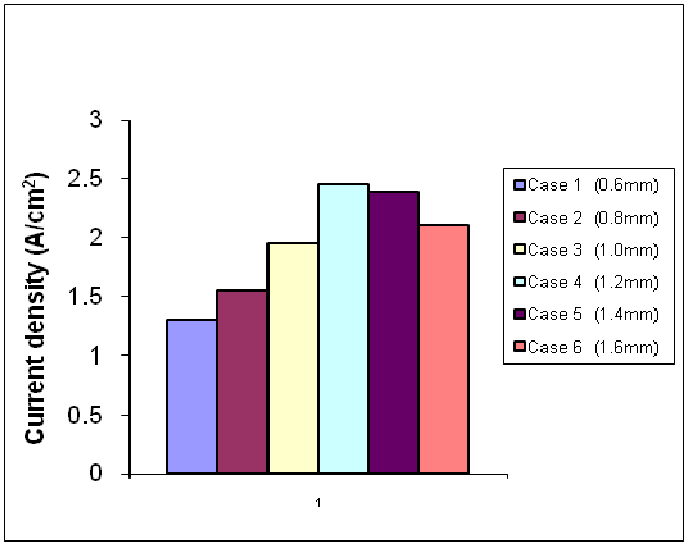

Figure 7 Current density obtained at different channel width at cell potential 0.4 V and temperature 70 ^{0}C.

Effect of GDL porosity

The effect of the GDL porosity on the performance of the PEM fuel cell is shown in Figure 8. The simulation result shows the fact that the effect of diffusion layer porosity on fuel cell performance is significant when the gas diffusion layer is in the low value region (0.1 to 0.3). Increasing the diffusion layer porosity size has an increasingly weaker effect on the performance. The gas diffusion layer porosity beyond 0.6 does not affect the fuel cell polarisation curve. Maintaining a porosity level between 0.4 and 0.5 will be a reasonable value for the fuel cell looking into durability issues in fuel cell structure.

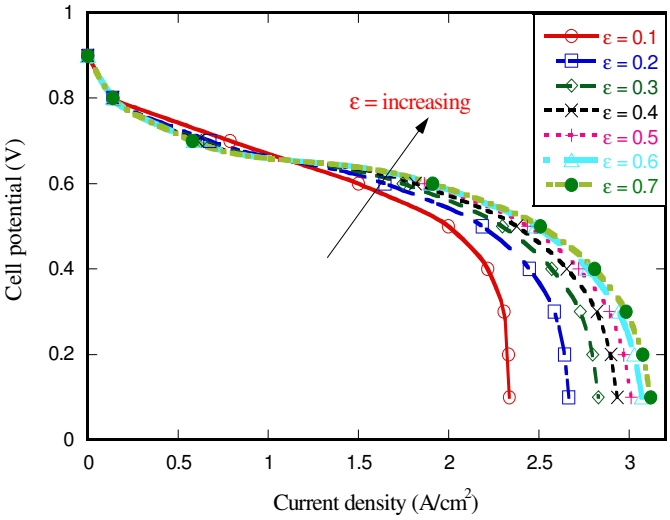

Figure 8 Effects of diffusion layer porosity at cell temperature of 70 ^{0}C.

Channel flow orientation

The effect of species flow orientation on the performance of the fuel cell was investigated at the base case. It was discovered that the direction of flow affects the performance of the fuel cells. The effect of co-flow and counterflow affects the fuel cell performance at different operating cell voltages. The fuel cell performance was examined at the base case conditions and channel depth and width of 2.0 mm and 1.2 mm, respectively, for the counterflow and the co-flow orientations. Current densities of 2.61 A/cm^2 and 2.54 A/cm^2 were obtained for the counterflow and co-flow cases, respectively. Counter-flow creates better performance for the fuel cell especially at higher current voltages. Figures 9a and Figure 9b show the contours of mass fraction for hydrogen at the anode for counterflow and co-flow cases, respectively. The contour shows that counterflow configurations allows more uniform distribution of the hydrogen species at the anode flow channel, which subsequently improves the performance of the fuel cell. The effective species distribution generally aids reaction on the membrane sites and this leads to increased current density.

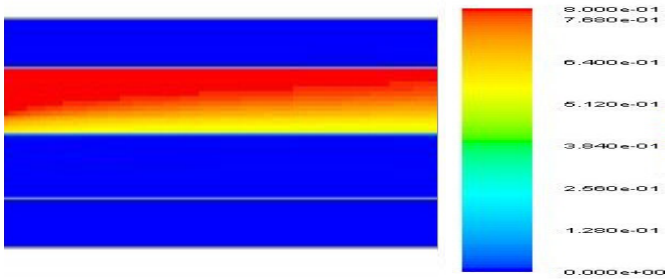

Figure 9a Contours of mass fraction of hydrogen at anode for counterflow case at the base case operating condition.

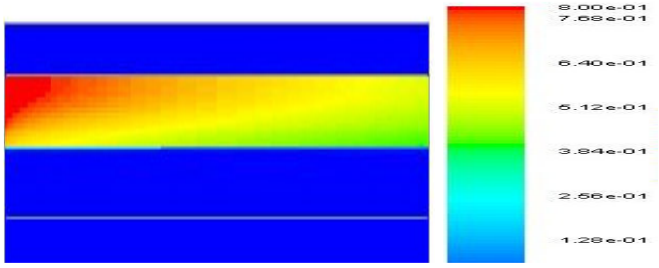

Figure 9b Contours of mass fraction of hydrogen at anode for co-flow case at the base case operating conditions.

CONCLUSION

An appropriate design of the fuel cell flow channels can significantly impact its performance. Numerical simulations were performed using the commercial computational fluid mechanics software Fluent® 12.0 with fuel cell add-on package for different channel depth, width and flow orientations. It was found that the optimum channel depth and width exist at 2.0 mm and 1.2 mm, respectively, for the model studied. The porosity effect has a significant effect on the PEM fuel cell especially in value ranges from 0.1 to 0.3. Gas diffusion layer porosity of between 0.4 and 0.5 will be appropriate for efficient performance of the fuel cell. Also, it was observed that counterflow orientation results in more even distribution of the reactant species at the anode better than co-flow orientation. The use of such channels with proper dimensions will lead to better performance of single-channel fuel cells. The model prediction is validated by comparison with experimental data in the open literature and was found to be in agreement. The numerical results provided useful information on the effect of the examined design and physical parameters on fuel cell performance**.**

Acknowledgment

The authors acknowledge the support of the Department of Mechanical and Aeronautical Engineering, University of Pretoria, the National Research Foundation and the Solar Hub funding from the University of Stellenbosch, via the Department of Energy.

References

[1] M. Arita, Technical issues of fuel cell systems for automotive applications. Yokosuka, Japan: Nissan Motor Co. Ltd.; 2002.
[2] D.M. Bernardi, Water balance calculations for solid polymer electrolyte fuel cells, J. Electrochem. Soc. 137 (11) (1990) 3344-3345.
[3] D.M Bernardi, M.W. Verbrugge, Mathematical model of gas diffusion electrode bonded to a polymer electrolyte, AIChE J. 37 (8) (1991) 1151-1163.
[4] T.E. Springer, T.A. Zawodzinski, S. Gottesfeld, Polymer electrolyte fuel cell model, J. Electrochem. Soc. 138 (8) (1991) 2334-2342.

[5] C. Xu, T.S. Zhao, A new flow field design for polymer
[6] J. Labaek, M. Bang, Flow and pressure distribution in fuel cell manifolds, ASME J. Fuel Sci. Technol., 7, p. 061001-1.
[7] S. Shimpalee, S. Greenway, J.W. van Zee, The impact of channel path length on PEMFC flow-field design, J. of Power Sources, 160, 398-406, 2006.
[8] S. Greenway, S. Shimpalee, J.W. van Zee, Presented at the 21st Meeting of the Electrochemical Society, Philadelphia, PA, May 2002.
[9] P.W. Li, S.P. Chen, M.K. Chyu, J. Power Sources 140 (2005) 311-318.
[10] X. Li, I. Sabir, J. Park, A flow channel design procedure for PEM fuel cells with effective water removal, J. Power Sources 163 (2007) 933-942.
[11] H. Ju, H. Meng, C.Y. Wang, A single-phase, non-isothermal model for PEM fuel cells, Int. J. Heat Mass Transfer 48 (2005) 1303-1315.
[12] S. Dutta, S. Shimpalee, J.W. van Zee, Numerical prediction of mass exchange between cathode and anode channels in a PEM fuel cell, Int. J. Heat Mass Transfer 44 (2001) 2029-2042.
[13] F. M. White (1986). Fluid Mechanics, second ed., New York: McGraw Hill.
[14] F. M. White (1991). Viscous Fluid Flow, New York: McGraw Hill. pp. 119-122.
electrolyte-based fuel cells, J. Elecom. (9) (2007) 497-503.
[15] Ansys Fluent® 12.0. (2009). Users Guide Documentation, Ansys Inc., Southpointe, SAS.
[16] S. V. Pantakar (1980). Numerical Heat Transfer and Fluid Flow, New York: Hemisphere Publishing Corp.
[17] W.Q., Tao, C.H. Min, X.L. Liu, Y.L. He, B.H. Yin, W. Jiang, Parameter sensitivity examination and discussion of PEM fuel cell simulation model validation Part I. Current status of modeling research and model development, J. Power Sources 160 (2006) 359-373.
[18] L. Wang, A. Husar, T. Zhou, H. Liu, A parametric Study of PEM fuel cell performance, Int. J. Hydrogen Energy 28 (2003) 1263-1272.
[19] C.H. Cheng, H.H. Lin, G. Lai, Design for geometric parameters of PEM fuel cell by integrating computational fluid dynamics code with optimisation method, J. Power Sources 165 (2007) 803-813.
[20] T. Berning, N. Djilali, J. Electrochem Soc. 150 (12) (2003) A1598-A1607.
[21] D.S. Watkins, K.W. Dircks, D.G. Epp. (1991). Novel fuel cell fluid flow field plate, US Patent 4988583.